PRESYNAPTIC NETWORKS

Single-cell–initiated monosynaptic tracing reveals layer-specific cortical network modules

Adrian Wertz,[1]* Stuart Trenholm,[1]* Keisuke Yonehara,[1] Daniel Hillier,[1] Zoltan Raics,[1] Marcus Leinweber,[1] Gergely Szalay,[2] Alexander Ghanem,[3] Georg Keller,[1] Balázs Rózsa,[2] Karl-Klaus Conzelmann,[3] Botond Roska[1,4]†

Individual cortical neurons can selectively respond to specific environmental features, such as visual motion or faces. How this relates to the selectivity of the presynaptic network across cortical layers remains unclear. We used single-cell–initiated, monosynaptically restricted retrograde transsynaptic tracing with rabies viruses expressing GCaMP6s to image, in vivo, the visual motion–evoked activity of individual layer 2/3 pyramidal neurons and their presynaptic networks across layers in mouse primary visual cortex. Neurons within each layer exhibited similar motion direction preferences, forming layer-specific functional modules. In one-third of the networks, the layer modules were locked to the direction preference of the postsynaptic neuron, whereas for other networks the direction preference varied by layer. Thus, there exist feature-locked and feature-variant cortical networks.

In the cortex, many neurons selectively respond to distinct environmental features such as image motion in a specific direction or orientation (*1*, *2*), the spatial position of the animal (*3*), or a specific part of a face (*4*). Each cortical neuron receives input from hundreds of nearby neighbors. Understanding the feature preference of the cortical neurons that provide input to a neuron with an identified feature preference could help us to understand how selectivity emerges and how cortical circuits are organized.

Within layer 2/3 of mouse primary visual cortex (V1), there is a close relation between orientation selectivity and synaptic connectivity (*5*). In contrast, in vivo single-cell recordings from layer 2/3 pyramidal cells in V1 have revealed different degrees of similarity between the preferred orientations at the dendritic input sites and at the cell body (*6*–*8*). The variability of orientation preferences at dendritic input sites could arise from differently tuned inputs from deeper cortical layers. The relation between the feature selectivity of the postsynaptic cell and the feature selectivity and functional organization of the deeper cortical neurons that provide synaptic input to individual layer 2/3 cells is still unknown.

We combined functionalized transsynaptic tracing with two-photon imaging and recorded the visually evoked responses of individual layer 2/3 pyramidal neurons together with their presynaptic neuronal networks across different cortical layers in vivo in mouse V1. Single-cell–initiated monosynaptic tracing (*9*) allows the expression of genetic tools in individual cortical neurons together with their monosynaptically connected presynaptic partners (*10*). This form of tracing is based on the delivery of three plasmids to a single neuron (one expressing a fluorophore, one expressing the avian receptor TVA, and one expressing the rabies virus envelope glycoprotein) and the local infection with the glycoprotein gene–deleted rabies virus coated with envelope-A [(EnvA), the ligand for the TVA receptor]. The EnvA-TVA ligand-receptor interaction restricts rabies virus infection to the TVA-expressing starter cell, and the glycoprotein allows rabies virus to move transsynaptically in the retrograde direction to only those neurons that monosynaptically connect to the starter cell (*9*). Rabies virus can be engineered to express genetically encoded calcium sensors, allowing the activity of the infected neurons to be recorded. The single-cell–initiated tracing system has been used for anatomical studies (*9*, *11*, *12*), but not yet for functional analyses.

Our modified version of single-cell–initiated monosynaptic tracing (*9*) differed in two aspects from previous approaches (Fig. 1A and supplementary materials and methods). First, we electroporated starter cells with four plasmids instead of three; the fourth plasmid, expressing a genetically encoded calcium sensor (GCaMP6s) (*8*), was necessary to record responses from the electroporated starter neuron. Second, we used a new rabies virus variant expressing GCaMP6s (materials and methods), which allowed for monitoring the activity from many presynaptic cells around the starter cell in a region spanning from layer 2/3 to layer 5. In each mouse, we labeled only a single layer 2/3 cell and its presynaptic network (Fig. 1B). We identified V1 using intrinsic in vivo imaging (*13*) (Fig. 1B and fig. S1) or post hoc confocal imaging in fixed brain slices (fig. S2). Soon after electroporation and rabies virus injection, the starter cell exhibited fluorescence (Fig. 1B). All starter cells were pyramidal cells. Next, presynaptic neurons expressing GCaMP6s appeared around the starter cell and increased in number as a function of time, whereas the responsiveness of the starter cell decreased as a function of time (Fig. 1, C and D, and fig. S3). Functional responses from presynaptic cells could be recorded up to ~2 weeks after electroporation, whereas starter cell responses could be recorded for ~1 week.

The total number of cells labeled in a presynaptic circuit, determined post hoc in immunostained brain slices, was 417 ± 74 (ranging from 70 to 846 cells, $n = 9$ presynaptic networks). The most abundant cluster of presynaptic cells surrounded the starter cell and was distributed across cortical layers (332 ± 64 presynaptic cells, ranging from 58 to 729 cells, $n = 9$) (Fig. 1, E to G, and fig. S4) (*14*). Within this local cluster, 82.5 ± 2.4% of cells were pyramidal cells (*15*). Outside of the local cluster of cortical neurons surrounding the starter cell, presynaptic cells were consistently labeled in several other brain regions that provide input to V1 (*14*) (fig. S5).

To determine the visual responses from the starter cell and its presynaptic network in V1, we presented animals with gratings that moved in eight directions and imaged GCaMP6s fluorescence with a two-photon laser scanning microscope from single optical planes with an area of 300 μm by 400 μm, from 40 to 600 μm below the brain surface, at 15- to 20-μm steps (Fig. 2A). Here we present functional data from 17 presynaptic networks connected to single pyramidal cells. From seven of these networks, in which the starter cell was electroporated with the four plasmids, we obtained visual motion responses from both the starter neuron and the presynaptic network. From 10 of the networks, electroporated with the three-plasmid approach (*9*), we obtained recordings from the presynaptic networks but not from the starter cells.

We imaged 98 ± 16 presynaptic cells in each presynaptic network. Nearly half (43 ± 4%) of these cells showed responses to image motion. Responses to motion were quantified using a direction-selective index (DSI) and an orientation-selective index (OSI) (calculated based on the vector sum of responses in all directions) (*16*) (fig. S6 and materials and methods). All presynaptic networks contained both direction- and orientation-selective neurons, and the degree of direction and orientation selectivity varied from neuron to neuron within a given network (Fig. 2, B to D, and fig. S6). Therefore, we analyzed all presynaptic networks for both direction and orientation selectivity.

Neurons within a single presynaptic network could be tuned to similar or different directions and orientations. We quantified the variability

[1]Neural Circuit Laboratories, Friedrich Miescher Institute for Biomedical Research, Basel, Switzerland. [2]Two-Photon Imaging Center, Institute of Experimental Medicine, Hungarian Academy of Sciences, Budapest, Hungary. [3]Max von Pettenkofer-Institute and Gene Center, Ludwig-Maximilians-University Munich, Munich, Germany. [4]Department of Ophthalmology, University of Basel, Basel, Switzerland.
*These authors contributed equally to this work. †Corresponding author. E-mail: botond.roska@fmi.ch

of the preferred directions and orientations of neurons within each of the 17 presynaptic networks. We determined the circular variance of the preferred directions and orientations in each of the presynaptic networks and estimated the probability that this variance could be obtained if equal numbers of neuronal responses were drawn randomly from a pool of responses measured using bulk rabies virus injection to V1 (Fig. 2, E to G; figs. S7 and S8; materials and methods). In 5 of the 17 presynaptic networks, the circular variance was significantly lower than the circular variances of the randomly chosen neuronal sets ($P < 0.01$) (Fig. 2G). We additionally performed two different statistical tests. First, the cumulative distributions of preferred directions and orientations in these five presynaptic networks were significantly different from the cumulative distribution of the pool of all responses (Kolmogorov-Smirnov test, $P < 0.05$) (fig. S9). Second, the hypothesis that the preferred directions and orientations of neurons within a presynaptic network were drawn randomly from a uniform distribution was

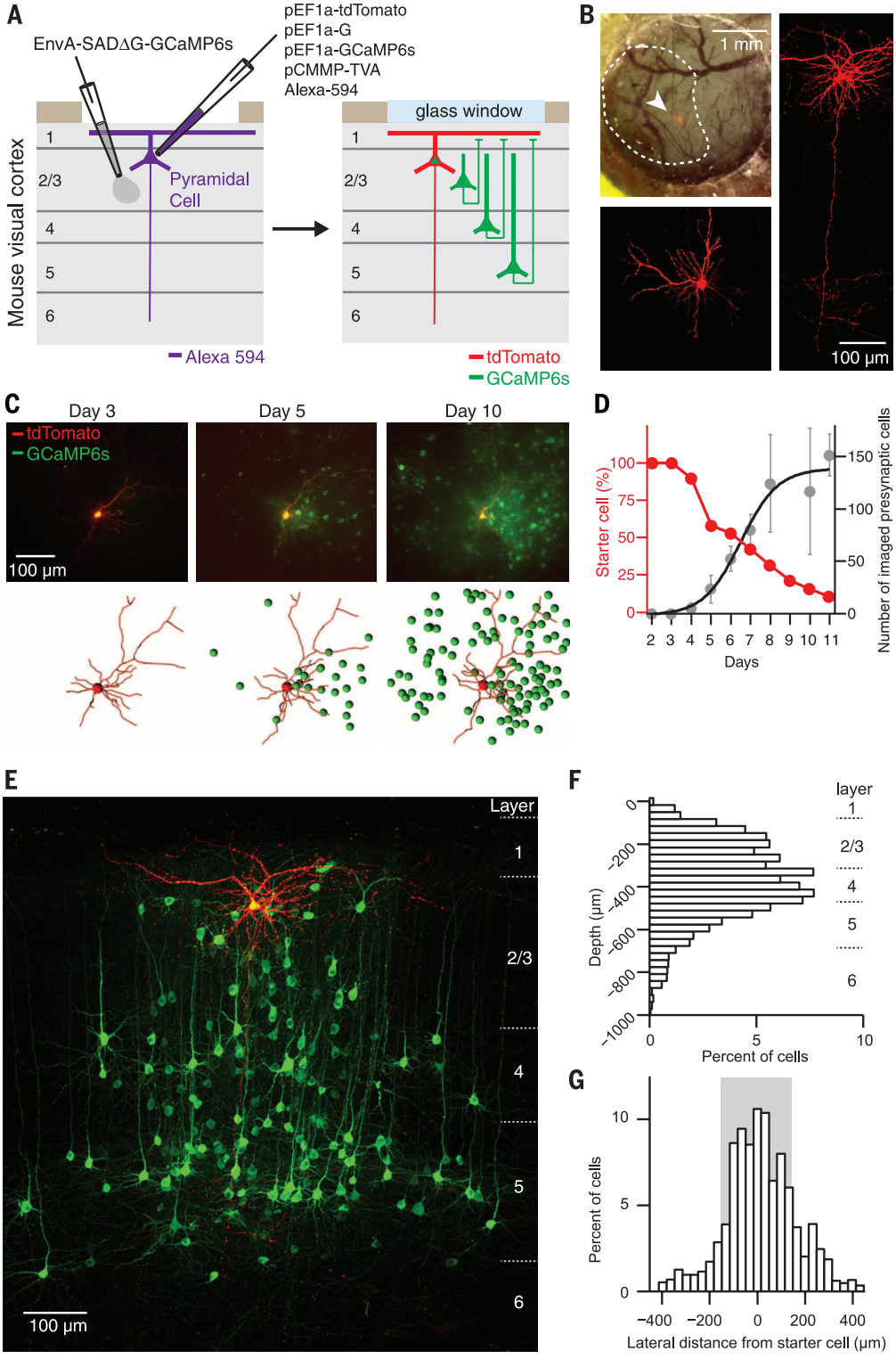

Fig. 1. GCaMP6s-functionalized, single-cell–initiated circuit tracing in mouse primary visual cortex. (**A**) Schematic of the experimental design. Individual layer 2/3 pyramidal cells in V1 were electroporated with a combination of four plasmids and Alexa 594 (purple) using the shadow-imaging technique (*26*, *27*). Immediately after electroporation, EnvA-SADΔG-GCaMP6s rabies virus was injected near the electroporation site. After a few days, the electroporated cell expressed tdTomato (red) and GCaMP6s (green), whereas its presynaptic neurons expressed only GCaMP6s. (**B**) A tdTomato-expressing electroporated starter cell is shown in a cranial window using epifluorescence imaging (top left), two-photon imaging (bottom left), and post hoc confocal imaging (right). The dotted line (top left) represents the boundary of V1, as determined with intrinsic optical imaging (fig. S1 and materials and methods). (**C**) *z* projections of two-photon image stacks (top) and reconstructions (bottom) of an electroporated starter cell (red) and its local presynaptic neurons (green) over an 8-day period. (**D**) The presence of the electroporated starter cell (red) and the number of local presynaptic neurons (gray) imaged in vivo with a two-photon microscope at different days after electroporation ($n = 15$ networks; error bars indicate SEM). The black curve is a sigmoid fit to the mean number of presynaptic neurons over time. (**E**) Confocal image of an electroporated layer 2/3 pyramidal cell (red) and its local presynaptic network (green) after antibody staining (image is from a 300-μm-thick slice). (**F**) Average depth distribution of cell bodies of presynaptic neurons across cortical layers ($n = 9$). (**G**) Average distribution of the lateral distance between the cell bodies of the starter cell and its presynaptic cells in V1 ($n = 5$). The gray shaded area indicates the region from which we performed in vivo two-photon imaging. Both (F) and (G) are based on post hoc confocal analysis.

rejected (Hodges-Ajne test, $P < 0.05$) (fig. S9). Therefore, about one-third of all studied presynaptic networks (5/17) were "tuned": the responding neurons had similar preferred directions and orientations. However, the majority of presynaptic networks (12/17) were "untuned": the preferred directions and orientations of the responding neurons did not significantly differ from random draws from the pool of bulk responses (Fig. 2, E to G, and fig. S10).

To understand the relation between the visual responses of the starter cell and its presynaptic network, we compared the preferred direction and orientation of the starter cell to the average preferred direction and orientation of the presynaptic network in all seven networks from which we obtained visual responses from both the starter cell and the presynaptic network. In all cases in which the presynaptic network was tuned (3/7), the average preferred direction and orientation of the presynaptic network were within a small range of angles relative to the preferred direction and orientation of the starter cell (direction: within 66 ± 22°; orientation: within 21 ± 11°; $n = 3$) (Fig. 3, A to C). Even in networks, which as a whole were untuned, layer 2/3 cells exhibited a bias such that they were tuned similarly to the starter neuron (direction: within 20 ± 10°; orientation: within 43 ± 13°; $n = 4$) (Fig. 3D and fig. S11).

Because layer 2/3 presynaptic subnetworks shared a similar preferred direction and orientation to the postsynaptic starter neuron, even in networks that were untuned, we analyzed the functional properties of presynaptic networks layer by layer. For each layer, we aligned the preferred direction and orientation of each neuron relative to the preferred direction and orientation of the layer subnetwork. We then averaged the aligned distributions layer by layer across all 12 untuned networks. Each layer subnetwork was significantly biased toward a single preferred direction and orientation [one-way analysis of variance (ANOVA), $P < 0.01$] (Fig. 3E and fig. S12). Additionally, the circular variances of these relative direction and orientation distributions of layer 2/3 and layer 4 subnetworks were significantly lower than the circular variances of randomly chosen response sets from the pool of responses within the same layer obtained by bulk injection; this was also true when compared with the pool of all responses obtained by bulk injection ($P < 0.05$) (fig. S13). The Kolmogorov-Smirnov test and the Hodges-Ajne test were significant for layers 2/3, 4, and 5 ($P < 0.05$) (fig. S13). These results suggest the existence of functional layer modules within presynaptic networks.

We next investigated, in untuned networks, how the preferred direction of layer modules shifted from layer to layer. There was no significant bias in direction preference of layer 4 or 5 modules with respect to that of layer 2/3 modules (one-way ANOVA, $P > 0.05$) (Fig. 4, A and B, and fig. S14).

So far, the results we have presented were based on successively imaging individual optical

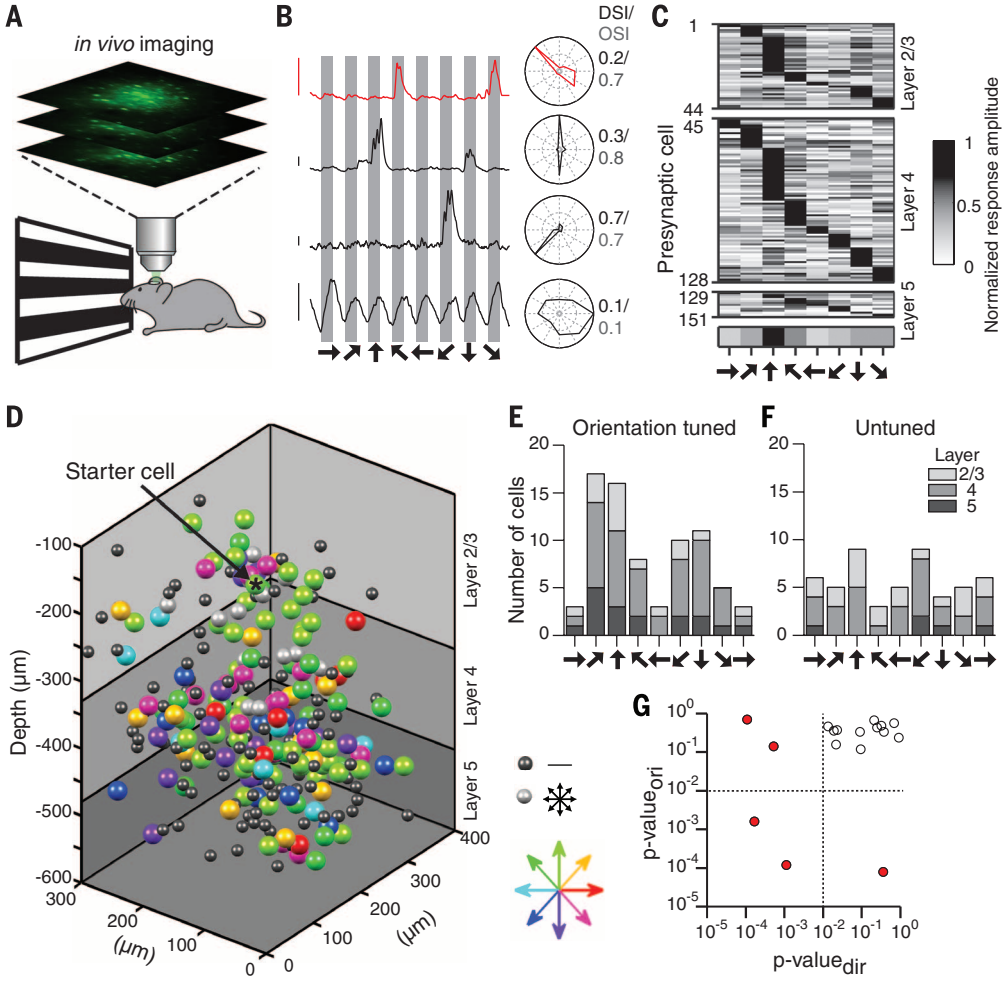

Fig. 2. Functional imaging reveals the existence of tuned and untuned presynaptic networks. (**A**) Schematic of the experimental protocol, in which mice were presented with moving gratings drifting in eight directions. GCaMP6s calcium responses were measured with a two-photon laser scanning microscope from different depths. (**B**) Example GCaMP6s responses from an electroporated starter cell (red) and three of its presynaptic neurons (black). Gray bars indicate when gratings were in motion, and arrows indicate the direction of stimulus motion. Polar plots of response amplitudes to each direction are shown to the right, as are the direction- and orientation-selective indices (DSI and OSI). Scale bars denote 100% $\Delta F/F$ (where F is fluorescence). (**C**) Raster plot for all cells with a DSI or OSI > 0.2 from an example network. Each horizontal line represents the normalized response amplitude of a single cell to eight directions of motion (shown below, scale bar at right). For each cortical layer (indicated on the right), cells are arranged based on the direction of motion driving the largest response. (**D**) Example 3D representation of the locations of a starter cell and its presynaptic neurons. Each filled circle represents a neuron and is colored according to the preferred motion direction (color code is shown at bottom right). Cells that did not respond to the visual stimuli are represented by small black circles. Cells that responded to motion equally in all directions are represented by small gray circles. (**E**) Distribution of the preferred motion directions in a representative tuned network. (**F**) Distribution of the preferred motion directions in a representative untuned network. (**G**) Plot of the P values of the circular variance of preferred directions ($p\text{-value}_{dir}$) and orientations ($p\text{-value}_{ori}$) of each network, calculated by comparing responses in each network to a randomly drawn set of responses from a pool (materials and methods). The dotted lines represent $P = 0.01$, with red dots indicating tuned networks.

planes in V1. To test whether the tuning of a presynaptic network was conserved if the activity of the three-dimensional (3D) network was imaged nearly simultaneously, we used a 3D acousto-optic two-photon microscope to measure network activity (*17*). We found no significant difference (Kolmogorov-Smirnov test, $P = 0.93$) in the overall motion direction preferences of networks when their activity was measured one optical plane at a time versus when the network was imaged in 3D in real time (fig. S15).

In summary, we used functionalized single-cell–initiated, monosynaptically restricted transsynaptic tracing and two-photon imaging in V1

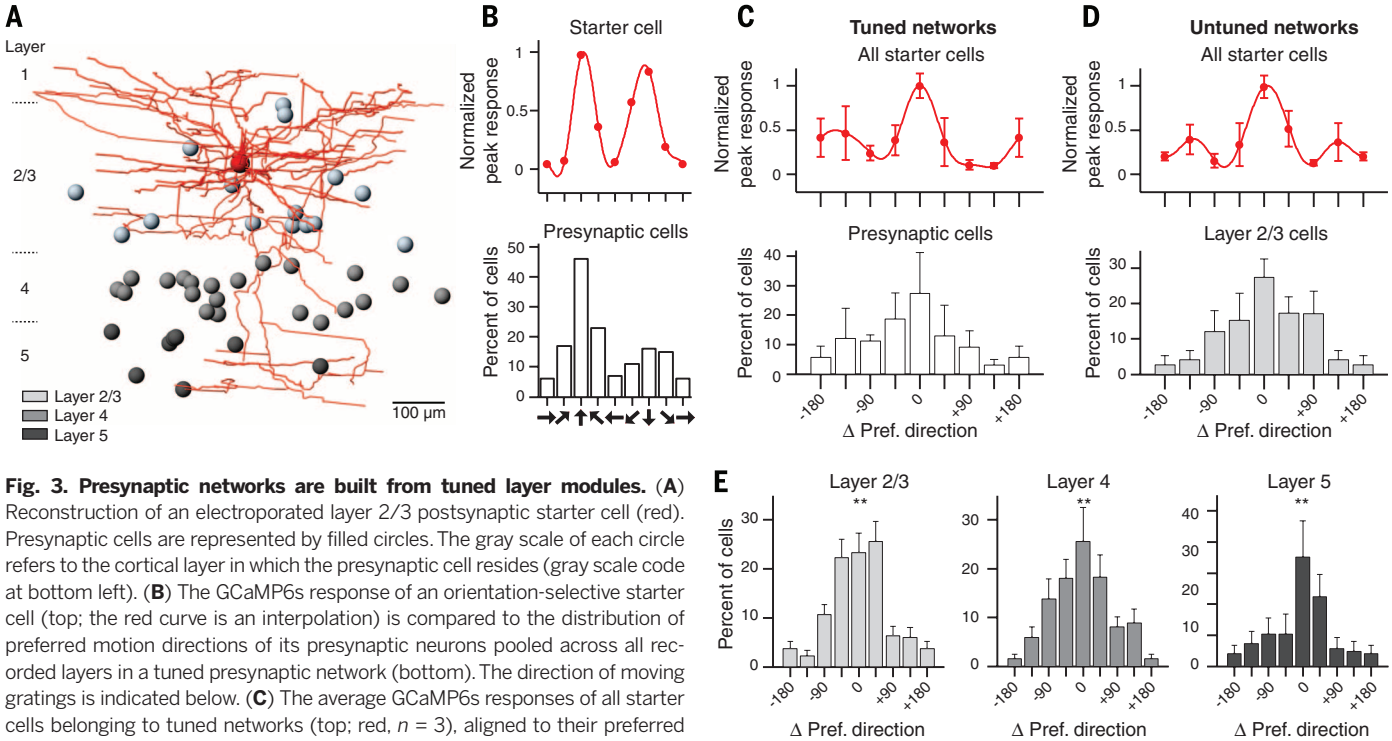

Fig. 3. Presynaptic networks are built from tuned layer modules. (**A**) Reconstruction of an electroporated layer 2/3 postsynaptic starter cell (red). Presynaptic cells are represented by filled circles. The gray scale of each circle refers to the cortical layer in which the presynaptic cell resides (gray scale code at bottom left). (**B**) The GCaMP6s response of an orientation-selective starter cell (top; the red curve is an interpolation) is compared to the distribution of preferred motion directions of its presynaptic neurons pooled across all recorded layers in a tuned presynaptic network (bottom). The direction of moving gratings is indicated below. (**C**) The average GCaMP6s responses of all starter cells belonging to tuned networks (top; red, $n = 3$), aligned to their preferred direction (the preferred direction was set to 0°), are compared to the relative preferred directions (relative to the preferred direction of the starter cell) of presynaptic neurons in these networks (bottom). (**D**) The average GCaMP6s responses of all starter cells belonging to untuned networks (top; red, $n = 4$), aligned to their preferred direction, are compared to the relative preferred directions of presynaptic neurons in layer 2/3 (bottom). (**E**) Distribution of relative preferred directions within layers (relative to the preferred direction of each layer subnetwork) in all untuned networks (materials and methods). The preferred direction of the layer subnetwork was set to 0°. $^{**}P < 0.01$ (one-way ANOVA). Error bars represent SEM.

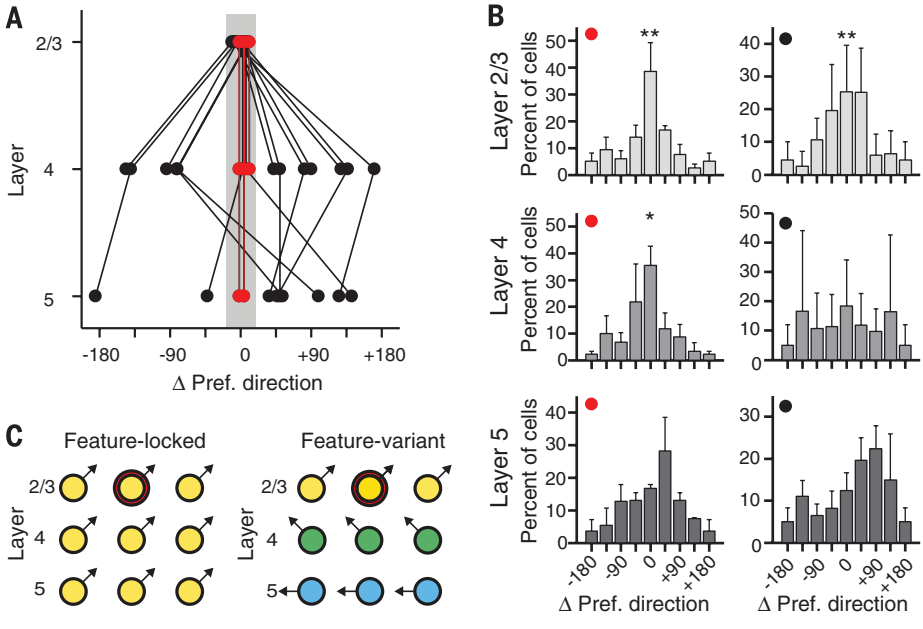

Fig. 4. Feature-locked and feature-variant networks. (**A**) In each of the 17 recorded networks, the preferred directions of layer modules were binned into eight directions (materials and methods) and are shown relative to the preferred direction of their layer 2/3 module. Solid lines link together the layer modules belonging to the same presynaptic network. Presynaptic networks that are tuned to the same direction across layers are indicated in red and highlighted by the gray shaded area. (**B**) Distributions of preferred directions of neurons in different cortical layers from networks in which each layer module was tuned to the same direction [left, red in (A)]. Preferred directions are shown relative to the preferred direction of the layer 2/3 module (materials and methods). Distributions of the preferred directions of neurons in different cortical layers from networks in which the preferred direction of each layer module was shifted compared with that of layer 2/3 [right, black in (A)]. $^{**}P < 0.01$; $^{*}P < 0.05$; one-way ANOVA. Error bars represent SEM. (**C**) Schematic representation of feature-locked (left) and feature-variant (right) networks. The starter cell is indicated with a red outline. The preferred direction of each neuron is indicated with an arrow.

to record the responses from individual layer 2/3 pyramidal cells together with their presynaptic partners in different cortical layers. Presynaptic cells within layers 2/3 and 4 (and, to some extent, layer 5) are tuned similarly for motion direction and orientation, forming layer-specific functional modules. The preferred direction and orientation of different layer modules can be aligned, resulting in presynaptic networks that are "feature-locked," or can be shifted relative to each other, giving rise to "feature-variant" networks (Fig. 4C).

The existence of feature-locked and feature-variant networks may explain why some studies found more variability than others in the tuning of dendritic input sites of layer 2/3 pyramidal cells (*6*–*8*) and may suggest that variability is likely due to inputs from deeper cortical layers. The combination of distinct layer modules in feature-variant networks is consistent with previous studies in brain slices showing cross-talk between different subnetworks in layer 2/3 and layer 5 (*18*, *19*). In the visual cortex, the strength of connections among neurons correlates with similarity in visual responses (*20*), raising the possibility that feature-locked networks have a higher density of strong connections compared with feature-variant networks. Also, whether different subtypes of cortical interneurons (*21*, *22*) are differentially represented in feature-locked and feature-variant networks remains an open question. Finally, it will be interesting to test whether postsynaptic cells in feature-locked and feature-variant networks exhibit different population coupling strengths (*23*).

What could be the role of feature-variant presynaptic networks? One possibility is that feature-variant networks are plastic. Top-down modulation or learning (*24*) could force the preferred direction and orientation of layer modules to align, resulting in a transition from a feature-variant to a feature-locked network. This recruitment of relevant circuits could allow more robust feature representations of behaviorally important stimuli. Another possibility is that variant layer modules enhance responses of the postsynaptic cell during object motion. Approaching and receding objects, for example, have edges moving in different directions. Some of these edges may stimulate inputs from deeper layers, which are not strong enough to drive responses of the postsynaptic cell alone but could boost responses of the postsynaptic cell to an edge moving in its preferred direction. Indeed, responses to combinations of orientations have been demonstrated in primate V2 (*25*).

REFERENCES AND NOTES

1. D. H. Hubel, T. N. Wiesel, *J. Physiol.* **148**, 574–591 (1959).
2. U. C. Dräger, *J. Comp. Neurol.* **160**, 269–290 (1975).
3. T. Hafting, M. Fyhn, S. Molden, M.-B. Moser, E. I. Moser, *Nature* **436**, 801–806 (2005).
4. W. A. Freiwald, D. Y. Tsao, M. S. Livingstone, *Nat. Neurosci.* **12**, 1187–1196 (2009).
5. H. Ko *et al.*, *Nature* **473**, 87–91 (2011).
6. S. L. Smith, I. T. Smith, T. Branco, M. Häusser, *Nature* **503**, 115–120 (2013).
7. H. Jia, N. L. Rochefort, X. Chen, A. Konnerth, *Nature* **464**, 1307–1312 (2010).
8. T.-W. Chen *et al.*, *Nature* **499**, 295–300 (2013).
9. J. H. Marshel, T. Mori, K. J. Nielsen, E. M. Callaway, *Neuron* **67**, 562–574 (2010).
10. I. R. Wickersham *et al.*, *Neuron* **53**, 639–647 (2007).
11. E. A. Rancz *et al.*, *Nat. Neurosci.* **14**, 527–532 (2011).
12. M. Vélez-Fort *et al.*, *Neuron* **83**, 1431–1443 (2014).
13. S. Schuett, T. Bonhoeffer, M. Hübener, *J. Neurosci.* **22**, 6549–6559 (2002).
14. Y.-J. Liu *et al.*, *Curr. Biol.* **23**, 1746–1755 (2013).
15. K. D. Harris, G. M. G. Shepherd, *Nat. Neurosci.* **18**, 170–181 (2015).
16. M. Mazurek, M. Kager, S. D. Van Hooser, *Front. Neural Circuits* **8**, 92 (2014).
17. G. Katona *et al.*, *Nat. Methods* **9**, 201–208 (2012).
18. B. M. Kampa, J. J. Letzkus, G. J. Stuart, *Nat. Neurosci.* **9**, 1472–1473 (2006).
19. Y. Yoshimura, J. L. M. Dantzker, E. M. Callaway, *Nature* **433**, 868–873 (2005).
20. L. Cossell *et al.*, *Nature* **518**, 399–403 (2015).
21. C. A. Runyan *et al.*, *Neuron* **67**, 847–857 (2010).
22. A. M. Kerlin, M. L. Andermann, V. K. Berezovskii, R. C. Reid, *Neuron* **67**, 858–871 (2010).
23. M. Okun *et al.*, *Nature* **521**, 511–515 (2015).
24. J. P. Gavornik, M. F. Bear, *Nat. Neurosci.* **17**, 732–737 (2014).
25. A. Anzai, X. Peng, D. C. Van Essen, *Nat. Neurosci.* **10**, 1313–1321 (2007).
26. K. Kitamura, B. Judkewitz, M. Kano, W. Denk, M. Häusser, *Nat. Methods* **5**, 61–67 (2008).
27. B. Judkewitz, M. Rizzi, K. Kitamura, M. Häusser, *Nat. Protoc.* **4**, 862–869 (2009).

ACKNOWLEDGMENTS

We thank R. da Silveira for helpful discussions about possible functional roles for feature-locked and -variant networks. We thank S. Oakeley and A. Drinnenberg for commenting on the manuscript and members of the Facility for Advanced Imaging and Microscopy at the Friedrich Miescher Institute (FMI) for assistance with anatomical data acquisition and image processing. Original data are curated and stored in the server of FMI. All materials described in this paper, with the exception of the rabies virus, can be obtained for noncommercial purposes after signing a material transfer agreement (MTA) with FMI. The rabies virus can be obtained for noncommercial purposes after signing an MTA with the Ludwig-Maximilians-University Munich. The plasmids can be obtained from Addgene (addgene.org). We acknowledge the following grants: Human Frontier Science Program Postdoctoral Fellowship (LT000173/2013) to S.T.; Japan Society for the Promotion of Science Postdoctoral Fellowship for Research Abroad to K.Y.; European Molecular Biology Organization Postdoctoral Fellowship to D.H.; Swiss National Science Foundation grant to G.K.; Swiss-Hungarian, Hungarian-French, Central-Hungarian Region, Research and Technological Innovation Fund and European Union 3x3D Imaging grants to B. Rózsa; German Research Foundation Neuronal Circuits grant (SFB 870) to K.-K.C. and A.G.; Gebert-Ruf Foundation, Swiss National Science Foundation, European Research Council, National Centres of Competence in Research Molecular Systems Engineering, Sinergia, Swiss-Hungarian, and European Union 3X3D Imaging grants to B. Roska. Author contributions: In vivo electroporation and virus tracing techniques were optimized by A.W. Experiments were designed by A.W., S.T., and B. Roska. Experiments were performed by A.W. and S.T. Image data analysis was performed by A.W. Immunohistochemistry was performed by A.W. and S.T. Morphological data analysis was performed by S.T. Stimulation software was written by Z.R. Two-photon microscopes were developed by B. Rózsa and optimized by G.S. and D.H. Rabies virus was developed by A.G. and K.-K.C. Plasmids were made by K.Y. The intrinsic imaging was performed by A.W., M.L., and G.K. The paper was written by A.W., S.T., and B. Roska.

SUPPLEMENTARY MATERIALS

www.sciencemag.org/content/349/6243/70/suppl/DC1
Materials and Methods
Figs. S1 to S15
References (*28*–*35*)

20 March 2015; accepted 29 May 2015
10.1126/science.aab1687

BRAIN STRUCTURE

Cortical folding scales universally with surface area and thickness, not number of neurons

Bruno Mota[1] and Suzana Herculano-Houzel[2,3]*

Larger brains tend to have more folded cortices, but what makes the cortex fold has remained unknown. We show that the degree of cortical folding scales uniformly across lissencephalic and gyrencephalic species, across individuals, and within individual cortices as a function of the product of cortical surface area and the square root of cortical thickness. This relation is derived from the minimization of the effective free energy associated with cortical shape according to a simple physical model, based on known mechanisms of axonal elongation. This model also explains the scaling of the folding index of crumpled paper balls. We discuss the implications of this finding for the evolutionary and developmental origin of folding, including the newfound continuum between lissencephaly and gyrencephaly, and for pathologies such as human lissencephaly.

The expansion of the cerebral cortex, the most obvious feature of mammalian brain evolution, is generally accompanied by increasing degrees of folding of the cortical surface into sulci and gyri (*1*). Cortical folding has been considered a means of allowing numbers of neurons in the cerebral cortex to expand beyond what would be possible in a lissencephalic cortex, presumably as the cortical sheet expands laterally with a constant number of neurons beneath the surface (*2*, *3*). Although some models have shown cortical convolutions

[1]Instituto de Física, Universidade Federal do Rio de Janeiro, Rio de Janeiro, Brazil. [2]Instituto de Ciências Biomédicas, Universidade Federal do Rio de Janeiro, Rio de Janeiro, Brazil. [3]Instituto Nacional de Neurociência Translacional, INCT/MCT, São Paulo, Brazil.
***Corresponding author. E-mail: suzanahh@gmail.com**

Science

Single-cell–initiated monosynaptic tracing reveals layer-specific cortical network modules

Adrian Wertz, Stuart Trenholm, Keisuke Yonehara, Daniel Hillier, Zoltan Raics, Marcus Leinweber, Gergely Szalay, Alexander Ghanem, Georg Keller, Balázs Rózsa, Karl-Klaus Conzelmann and Botond Roska

Science **349** (6243), 70-74.
DOI: 10.1126/science.aab1687

Tracing cells that project to one neuron

Feature extraction is a prominent characteristic of cortical neurons involved in the early stages of sensory processing. Wertz *et al.* retrogradely marked an injected neuron and its direct inputs to reveal the network mechanisms that mediate their response. Neurons within each presynaptic network layer of single direction-selective cells showed similar motion direction preferences. In some networks, layer-specific functional modules were identical to the orientation preference of the postsynaptic neuron. Presynaptic neurons, however, displayed a general bias toward the stimulus feature that elicited a response in the postsynaptic neuron.

Science, this issue p. 70